ISBN: 978-3-95450-205-9 doi:10.18429/JACoW-Cyclotrons2019-WEC01

CONCEPTUAL DESIGN OF CENTRAL REGION FOR HIGH-TEMPERATURE SUPERCONDUCTING SKELETON CYCLOTRON (HTS-SC)

H. W. Koay†, M. Fukuda, H. Kanda, M. Nakao, T. Yorita
Research Centre for Nuclear Physics (RCNP), Osaka University, Japan

Abstract

A compact high-current accelerator is highly desirable for short and effective Boron Neutron Capture Therapy (BNCT) as well as radioisotopes production in a hospital environment. In accordance with this, a compact high-temperature superconducting skeleton cyclotron (HTS-SC) was proposed. HTS-SC is an air-core K-80 cyclotron with a relatively small extraction radius of 40 cm for a 50 MeV H^+ and 40 MeV D^+ beam. Owing to its compactness, a relatively high central magnetic field (>2.4 T) remains as a significant challenge for high current injection. This work describes a preliminary study of the injection using a spiral inflector and the central region design of the HTS-SC. Besides, the transverse beam dynamics are also discussed in order to investigate the upper limit of injection current.

INTRODUCTION

Since the first cyclotron developed by E.O. Lawrence and M. S. Livingston [1], it has been widely applied in various scientific researches and applications. In accordance with the advancement of high-temperature superconducting (HTS) tapes since these decades, the performance of a HTS cyclotron had also improved greatly to be more compact and efficient in producing high-energy or high-intensity beam with a lower power consumption. Following this trend, many works around the world have adopted HTS cyclotrons in various medical applications. However, most of them are relatively bulkier and of low-intensity (<100 μA), as they are mostly used to produce radioisotopes [2, 3]. In order to improve the versatility of HTS cyclotrons for direct therapeutic applications such as particle therapy or BNCT, beams of higher intensity are necessary. Therefore, this work wishes to propose a HTS skeleton cyclotron (HTS-SC) to produce a high-intensity beam for the previously proposed accelerator-based multi-port BNCT (AB-mBNCT) system, which can deliver multiple treatments at the same time [4], as well as the production of medical radioisotopes. Figure 1 shows the schematic of the applications of HTS-SC.

The proposed HTS-SC is an air-core (i.e. meaning of "skeleton") K-80 cyclotron with a small extraction radius of 40 cm for multiple-ion beams. It consists of 3 sector coils (SC) with a maximum spiral angle of 40°, 1 circular main coil (MC) of 60 cm radius and 7 small trim coils (TC) of radius varying from 5 cm to 45 cm. Owing to its compactness, a relatively high central magnetic field of about 2.4 T is required for a 50 MeV H+ beam. The radio frequency system consists of two 90° Dee locating directly opposite to each other, presently operating at a frequency from 34.5 MHz to 75 MHz with a maximum voltage of about 80 kV. Besides, an external injection system is required for the proposed HTS-SC in order to produce a high-intensity beam. As a part of the study of HTS-SC, this work will discuss about the conceptual design of its central region and its corresponding injection using a spiral inflector. As the space-charge effect is very important for a high-intensity beam at low energy, the transverse beam dynamics from the entrance of the inflector until several tenths of turns in the cyclotron are also discussed in order to investigate the upper limit of the injection current.

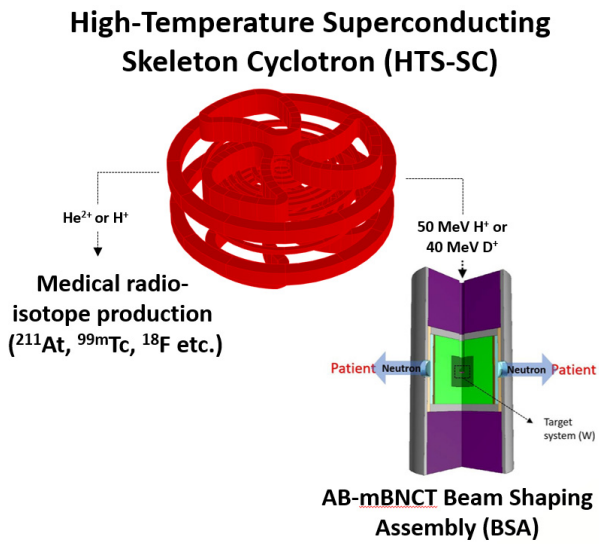

Figure 1: Schematic of the proposed HTS-SC and its application for AB-mBNCT as well as radioisotope production.

MATERIAL AND METHOD

Magnetic Field Distribution

The magnetic field distribution was calculated using the finite element magnetostatic (FEM) code TOSCA. The isochronous field is first estimated using Eq. (1).

$$< B(\bar{r}) > = \frac{B_o}{\sqrt{1-\beta(\bar{r})^2}} \quad (1)$$

After that, a better isochronous field was optimized by utilizing the orbital frequency obtained from OPAL (Object Oriented Parallel Accelerator Library) code developed by PSI [5]. The radial dependence of average magnetic field after optimization of isochronism is shown in Fig. 2.

ISBN: 978-3-95450-205-9 doi:10.18429/JACoW-Cyclotrons2019-WEC01

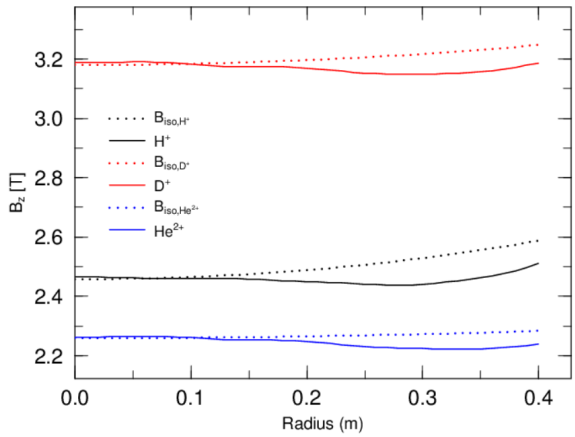

Figure 2: Average magnetic distribution for H^+ (black), D^+ (red) and He^{2+} (blue) ions up to 40 cm. Dotted lines show the analytical estimation of isochronous field using Eq. 1.

Central Region and Spiral Inflector

In order to inject the particles into median plane of HTS-SC, an inflector is needed. This work adopted a spiral inflector due to it is small-size and a relatively lower electric potential than other of the same kind. After considering the offset of beam at the inflector exit and the mechanical limitation of the bending structure, 40 keV was finally chosen as the injection energy. Table 1 shows the optimized parameters of the spiral inflector proposed in this study. Figure 3 shows the 3D CAD drawing of the spiral inflector and the central region of the HTS-SC. The average electric field distribution along the beam trajectory simulated by TOSCA is shown in Fig. 4.

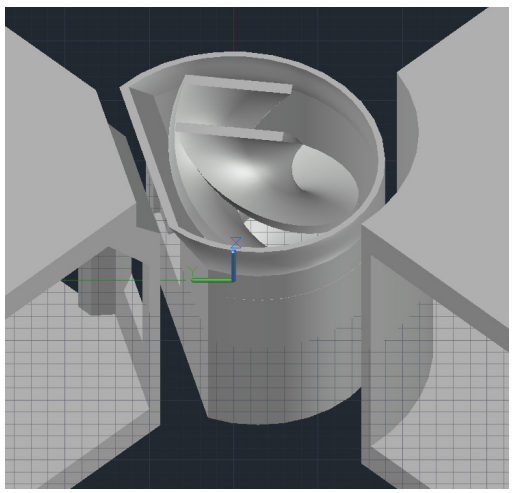

Figure 3: The 3D CAD drawing of the spiral inflector with the RF shield in the central region of HTS-SC.

RESULTS AND DISCUSSIONS

All the single-particle analysis and beam dynamics discussed in this work were performed by using SNOP developed by Victor Smirnov et al. [6]. Only single H^+ particle is involved in the following analysis, as this is the most important primary beam for AB-mBNCT neutron source. The injection was assumed to be at 40 mm above the median plane, which is 4 mm above the entrance plane of the inflector.

Table 1: Optimised Parameters of the Spiral Inflector

Parameter	Value
Beam Energy	40 keV
Tilt (k')	0.17
Inflector Height (A)	3.6 cm
Electric Field (E_u)	20.93 kV/cm
Electrode gap (entrance)	8 mm
Aspect ratio (ξ)	2

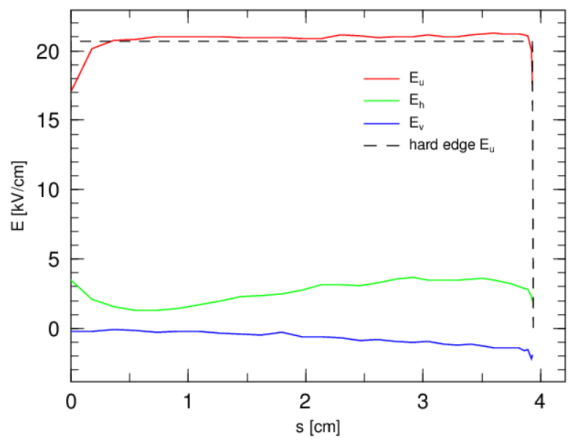

Figure 4: The electric field $\vec{E}$ directed in $\hat{u}$ (red), $\hat{h}$ (green), $\hat{v}$ (blue) along the beam trajectory simulated by TOSCA. The black dashed line represents the analytical hard edge E_u.

Single Particle Tracking

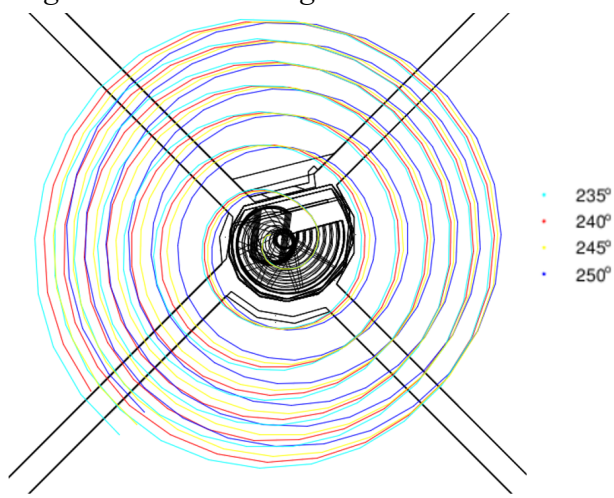

Figure 5: The accelerated orbits of H^+ ions from 40 keV to about 1.4 MeV with starting phases at 235° (cyan), 240° (red), 245° (yellow) and 250° (blue) respectively.

Beam Trajectory Simulations of the single particle tracking from injection above the inflector until the 6th turn were performed to show the feasibility of the design. The trajectory of the H^+ ion from 40 keV to 1.4 MeV with different starting phases from 235° to 250° at the median plane

ISBN: 978-3-95450-205-9 doi:10.18429/JACoW-Cyclotrons2019-WEC01

of the central region and the accelerating gaps are shown in Fig. 5.

Energy Gain Figure 6 shows the energy of the H^+ particle with an initial phase of 245°. Although the energy gain during the first 3 turns is just ~80% of the maximum energy gain due to the central bump of the magnetic field, this phase lag is reduced and almost fully recovered at the 6th turn. Also, the particle is crossing the gap when the electric potential is reducing. This enhances the axial focusing due to the Einzel focusing of the electric field.

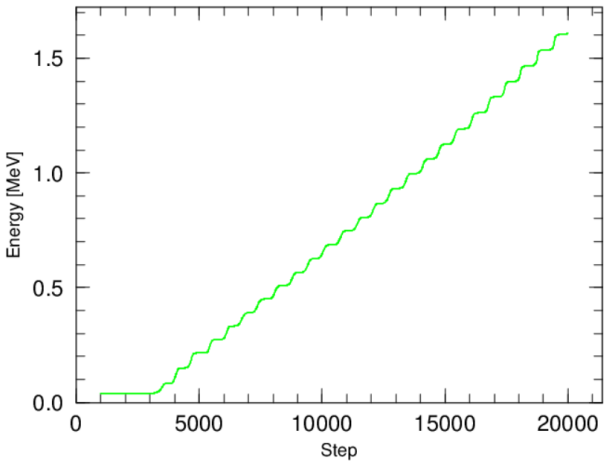

Figure 6: The energy gain of the H+ particle from 40 keV to about 1.6 MeV (up to the 6th turn).

Motion of Orbit Center Figure 7 shows the motion of the orbit centre to the 36th turn for particles of injection phases of 240˚, 245˚ and 250˚, respectively. The results show that the offset of the orbit centre is well confined within ±10 mm. This can easily be corrected by introducing first harmonic component into the acceleration.

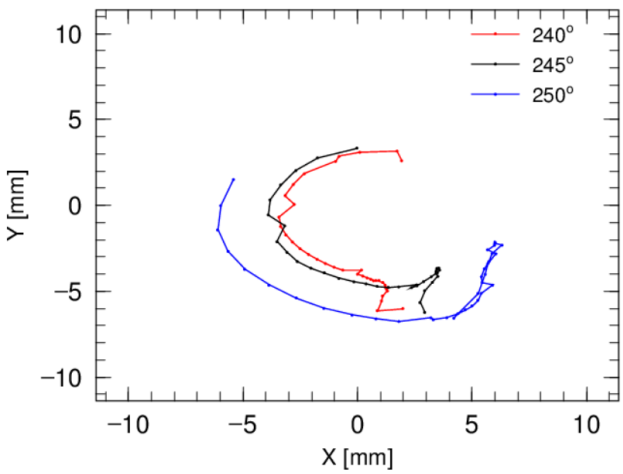

Figure 7: The motion of orbit centre (up to the 36th turn) in the central region for the particle with an injection phase of 240° (red), 245° (black) and 250° (blue) respectively.

Beam Dynamics

Beam Acceptance In order to determine the 6D phase acceptance of the central region (up to the 6th turn), an initial beam with (σ_x, σ_y) of (1.5 mm, 3 mm) and ($\sigma_{x'}$, $\sigma_{y'}$) of (30 mrad, 70 mrad) in trace spaces is generated at z = 40 mm. After passing through the spiral inflector, the particles which can survive up to the 6th turn gives the 6D beam acceptance of the injection system. However, as a spiral inflector couples the x-y motion of a particle, the acceptance contains x-y coupled component. This means that in order to perfectly match with the acceptance, an external beam skewer such as a quadrupole magnet is needed before injection into the spiral inflector. As far as this study is concerned, we are assuming a general injected beam without any coupling. Thus, only the projected beam acceptance is considered. The projected beam acceptance is about 29.8 π and 72 π mm·mrad in x and y direction respectively. The beam centre at the initial position in x-y real-space and x'-y' trace-space are shifted to (0.43 mm, 0.93 mm) and (2.9 mrad, -30.7 mrad) respectively due to the existence of fringing fields of the spiral inflector. Figure 8 shows the projected beam acceptance and the calculated rms emittance envelope.

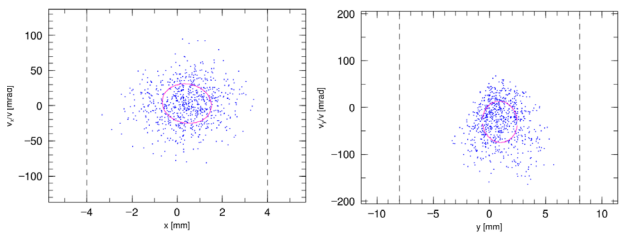

Figure 8: Projected beam acceptance of the central region of HTS-SC up to the 6th turn. The rms emittance bounded by the acceptance (pink line) is 29.8 π and 72 π mm·mrad in x and y respectively.

Current Dependence As the space charge effect is significant at low energy, the current dependence of the survival rate was also investigated. 3000 particles were injected (bounded by the projected acceptance shown in Fig. 8) from z = 40 mm. The surviving rate was then determined every 2000 step until the 36th turn in the cyclotron. The survival rate at different radii for different beam currents from 1 μA to 10 mA is shown in Fig. 9.

Generally, most of the particles are lost during the first turn (radius of < 30 mm) as they tend to hit the wall or ceiling of the Dee cavity. This kind of loss is magnified at high current owing to the existence of repulsive space-charge effect. This can be seen from the severe beam loss for the beam current of 5 mA (42%) and 10 mA (60%) during the first turn (r<30 mm). However, as particles accelerate, space charge effect is relieved and the beam loss is confined to be less than 10% until the 36th turn. This means that these particles are very likely to survive until extraction at the final turn. On the other hand, the beam loss of 1 μA, 0.1 mA and 1 mA are about 12%, 13% and 20% respectively up to 36th turn. This satisfactory result confirms the feasibility of the central region design for multi-particle motion.

ISBN: 978-3-95450-205-9 doi:10.18429/JACoW-Cyclotrons2019-WEC01

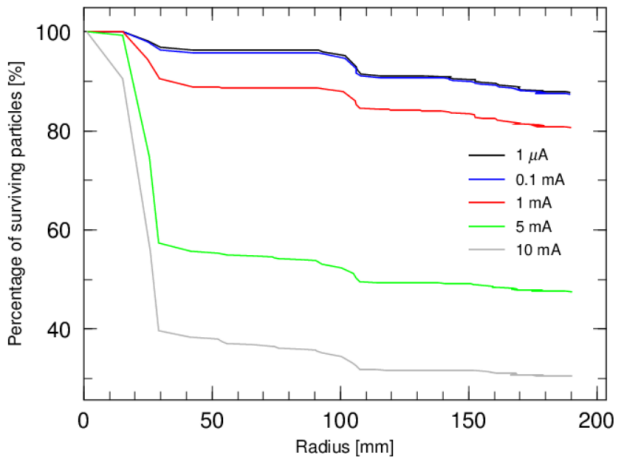

Figure 9: Percentage of surviving particles up to the 36th turn for beam current of 1 μA (black); 0.1 mA (blue), 1 mA (red), 5 mA (green) and 10 mA (grey) respectively.

Longitudinal Spread Besides the survival rate, the dependence of the longitudinal spread on to the space charge effect is also very important as the longitudinal spread of beam affects the beam resolution directly. Fig. 10 shows the longitudinal RMS spread for a 1 μA (Fig. 10(a)) and a 10 mA beam (Fig. 10(b)) up to the 36th turn for different initial rf phase width. As for the case of 1 μA beams, the longitudinal spread for a $\sigma_{rf} = 10^{o}$ is much wider than that of smaller width of 2.5 ° or 5°. However, this difference in rms is less significant for a 10 mA beam. This could be due to the enormous repulsive space charge effect that it overwhelmed any other causes, which could possibly increase the longitudinal spread of the beam. Besides, as the general trend, the rms difference in longitudinal direction due to different initial rf widths is becoming less significant as particles accelerate. This could be due to longitudinal bunching which might have taken place where particles that are lagged in phase are killed in the first few turns. This again proves our hypothesis that if particles can survive the first few turns, it is very likely for them to stay in the beam until the final turn, even for a high current beam.

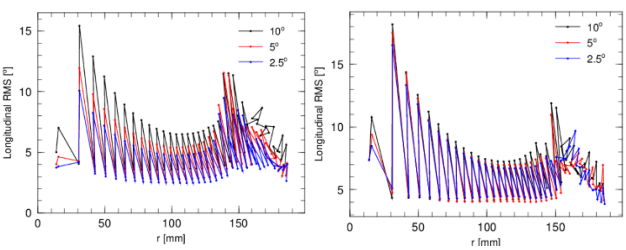

Figure 10: Longitudinal RMS spread for *left:* (a) 1μA, *right:* (b) 10 mA beam up to the 36th turn for initial rf phase width of σ_{rf}=2.5° (blue), 5° (red), and 10° (black) respectively at azimuthal position of 90° and 270°.

Transverse Beam Size As beam growth at the central region is significant, the radial and axial rms were also studied using different injection current from 1 μA up to 10mA. Figure 11 shows the average motion in z direction, while Fig. 12 shows the RMS beam size in radial and axial direction respectively.

From Fig. 11, the mean axial motion of the beam, including the particles within 1 σ in z direction, are well confined within the axial aperture of ±20 mm for beams of 1 μA to 10 mA. In fact, the average motion as well as the beam rms are similar for these three different beam currents. This again shows that space charge effect is the most significant only at the first two turns. If the particles managed to survive, they are very likely to be able to stay in the coasting beam until the final turn. Figure 12, which shows the beam rms in r and z direction, also confirms this statement due to the similar rms growth for different beam currents.

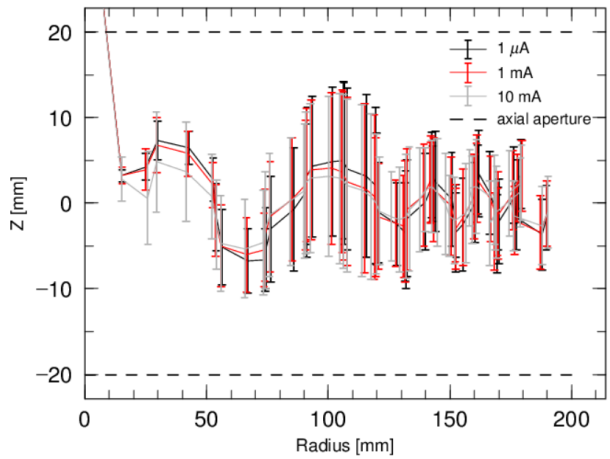

Figure 11: Average axial motion of the particles of beam current of 1 μA (black), 1 mA (red) and 10 mA (grey). Error bars represents 1 σ from the average trajectory.

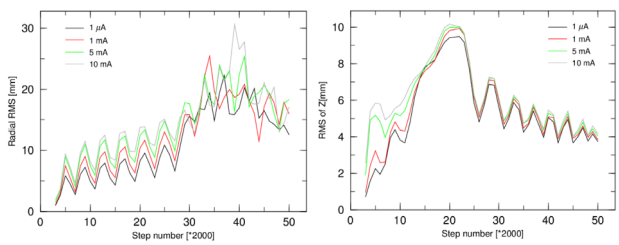

Figure 12: RMS (standard deviation) of the beam in radial (left) and axial (right) direction up to 36th turn. The beam current is 1 μA (black); 1 mA (red), 5 mA (green) and 10 mA (grey) respectively.

CONCLUSION

In conclusion, despite of the high central magnetic field of more than 2.4 T for H^+ beam, more than 80% of survival rate for a 1 mA beam is achieved by using the proposed spiral inflector of a high K value of >1.6. This satisfactory performance confirms the feasibility of the central region design in this work. Besides, this study also shows that most particles are killed during the first few turns. If we managed to increase the survival rate of the first few turns by introducing suitable coupling in x-y direction before injecting it into the inflector to improve the matching of the 6D acceptance, higher beam current is. Thus, additional elements such as a quadrupole magnet and an external buncher along the injection line shall remain as part of the next study. Furthermore, in order to confirm the survival

ISBN: 978-3-95450-205-9 doi:10.18429/JACoW-Cyclotrons2019-WEC01

rate of beams until extraction, the study of multi-bunch beam dynamics, coupled with the use of harmonic coils should also be performed in the coming future in order to check the neighbouring space-charge effect.

REFERENCES

[1] E. O. Lawrence and M. S. Livingston, "The Production of high speed light ions without the use of high voltages," *Physical Review,* vol. 40, no. 1, pp. 19-35, 1932. doi:10.1103/PhysRev.40.19

[2] A. E. Geisler *et al.*, "Commissioning of the Accel 250 MeV proton cyclotron", in *Proc. 18th Int. Conf. on Cyclotrons and Their Applications (Cyclotrons'07)*, Giardini-Naxos, Italy, Oct. 2007, pp. 9-14.

[3] V. Smirnov, S. Vorozhtsov, and J. Vincent, "Design study of an ultra-compact superconducting cyclotron for isotope production", *Nucl. Instrum. Methods Phys. Res., Sect. A*, vol. 763, no. 0168-9002, pp. 6-12, 2014. doi:10.1016/j.nima.2014.06.013

[4] H. W. Koay, M. Fukuda, H. Toki, R. Seki, H. Kanda, and T. Yorita, "Feasibility study of compact accelerator-based neutron generator for multi-port BNCT system," *Nucl. Instrum. Methods Phys. Res., Sect. A,* vol. 899, no. 0168-9002, pp. 65-72, 2018. doi:10.1016/j.nima.2018.05.025

[5] A. Adelmann, P. Calvo, M. Frey, A. Gsell, U. Locans, C. Metzger-Kraus, N. Neveu, C. Rogers, S. Russell, S. Sheehy, J. Snuverink, and D. Winklehner, "OPAL a versatile tool for charged particle accelerator simulations," *J. Comput. Phys.,* vol. arXiv preprint arXiv:1905.06654, 2019.

[6] V. L. Smirnov and S. B. Vorozhtsov, "SNOP – Beam dynamics analysis code for compact cyclotrons", in *Proc. 23rd Russian Particle Accelerator Conf. (RuPAC'12)*, Saint Petersburg, Russia, Sep. 2012, paper TUPPB008, pp. 325-327.